External Compression Supersonic Inlet Analysis Using a Finite Difference Two-Dimensional Navier-Stokes Code

A. F. Campbell,* J. Syberg,† and C. K. Forester†
Boeing Military Airplane Company, Seattle, Washington

Progress on the development and application of an analytical design procedure for the aperture region of two-dimensional external compression inlets is presented. The ultimate objective of the study is to derive from analysis additional design information that can be used to optimize external compression inlet performance. The major elements of the design procedure are a geometry generation code and a two-dimensional finite difference Navier-Stokes code. The results of a grid refinement study using the Navier-Stokes code are presented, as well as the results of a study of the effect of cowl lip spillage flow on ramp wall pressure distribution. Validation of the analysis is still in the preliminary stages. A comparison of analytical results with experimental data for one aperture region geometry at one operating point is given.

Nomenclature

M = Mach number
P = static pressure
P_T = total pressure
P_{TO} = supply plenum total pressure
W = mass flow
W_C = mass flow through inlet simulator capture area at supply nozzle exit
W_{spill} = subsonic mass flow spillage around cowl lip

I. Introduction

EXTERNAL compression inlets are used on several current supersonic aircraft. Consequently, a large amount of wind tunnel data on such inlets is available to guide the development of future systems. However, the data fail to explain exactly how the most critical region of the inlet (namely, the inlet aperture region) should be designed for optimum performance. This region, which is illustrated in Fig. 1, encompasses the cowl lip, the normal shock/boundary-layer interaction control device (e.g., a bleed slot), and the initial part of the diffuser. Aerodynamically, it is a highly complex flow region with normal shock(s), rapid expansion and flow turning, large transonic areas, and strong inviscid/viscous interactions. Both the internal performance and the inlet drag are strongly affected by the design of this area of the inlet.

The increasing cost of parametric model and full-scale testing, advances in numerical fluid mechanics, and rapid increases in computer speed and storage have led to the increased application of computational fluid dynamic (CFD) analysis in design concept evaluation studies. This paper presents progress on the development and application of an analytical design procedure employing CFD technology for the aperture region of two-dimensional external compression inlets. The ultimate objective of this study is to derive from analysis additional design information that can be used to optimize external compression inlet performance.

The major elements of the analytical design procedure are a geometry generation code and a two-dimensional finite difference Navier-Stokes code. An overview of these codes is provided in Sec. II. Validation of the design procedure is achieved using test data generated at the Boeing Diffuser Test Facility described in Sec. III. Results to date are presented in Sec. IV.

II. Code Description

The cowl lip, forward ramp, and aft ramp components of an external compression inlet are generated using an inlet geometry code. Output from the code serves as input to the two-dimensional Navier-Stokes code.

Inlet Geometry Code

The external compression inlet geometry code (ECIG) allows the user considerable flexibility in geometry definition. Surface contours are defined between user-specified control points by a cubic connecting function. A vector defining the surface slope and an associated relative magnitude is required at each control point location. The cubic connecting function defines the path of minimum change in slope between the initial and terminal control points within the constraints imposed by the user-specified control point slope vectors. The resulting path of minimum slope change defines the desired geometric surface.

The inner and outer initial control points of the cowl lip are defined by the endpoints of a half-ellipse that forms the tip or leading edge of the lip. The shape and orientation of the half-ellipse are required input information as are terminal control points defining the ends of the cowl lip. By varying the relative locations of the half-ellipse and the terminal control points, the amount of offset or total frontal area of the cowl lip is controlled. The orientation of the half-ellipse leading edge determines the deflection angle seen by the incoming flow. Control point slope directions at the initial and terminal point locations are fixed tangent to the surface at the half-ellipse and diffuser entry, respectively. The shape of the lip for a given offset is controlled by varying the relative magnitudes of the slope vectors at the initial and terminal control point locations. The mechanics of ECIG aperture region geometry generation are illustrated in Fig. 2.

Presented as Paper 84-1275 at the AIAA/SAE/ASME 20th Joint Propulsion Conference, Cincinnati, Ohio, June 11-13, 1984; received Aug. 4, 1984; revision received March 19, 1985.

*Senior Engineer.
†Senior Specialist Engineer.

The ramp surface is defined by the ramp angle and by initial and terminal control point locations and slopes. Again, slope directions are fixed tangent to the surface and relative magnitudes are varied to produce the desired curvature/shape. Bleed slot size and location is defined from station coordinates designating forward and aft ramp component locations.

In addition to geometry definition, ECIG generates surface curvature and area distribution information that allows a quantitative comparison of various lip and ramp shapes. A comparison of two inlet aperture region geometries is presented in Fig. 3.

Output from ECIG is in the proper format for input to the Navier-Stokes code. In addition, output from ECIG is compatible with other computer codes that generate shaded graphics displays and properly formatted files for communication to the shops for numerical-controlled (NC) machining.

Navier-Stokes Code

A two-dimensional Navier-Stokes code, P367, was selected to analyze the inlet aperture region flowfield because of its ability to model simultaneously the normal shock, flow spillage around the cowl lip, throat slot bleed flow, and flow turning through the forward part of the inlet. Obviously, three-dimensional effects such as the shock/boundary-layer interaction on the sideplates, corner spillage and sideplate bleed cannot be simulated using a two-dimensional code. Although three-dimensional Navier-Stokes codes are available, the cost of such an analysis is extremely high. Also, current computer storage capabilities limit the size of the three-dimensional mesh so that all flowfield phenomena cannot be adequately resolved within a single mesh. For these reasons, a two-dimensional analysis was chosen for the current study and only extensive comparison with experimental data can adequately determine the effect of the two-dimensional assumption on solution accuracy and resultant analysis design capability.

The two-dimensional Navier-Stokes code was originally written to solve nozzle/afterbody problems as described in Refs. 1-3. The explicit MacCormack algorithm is used to approximate the solution of the time-averaged, compressible Navier-Stokes equations. The algorithm utilizes time relaxation to obtain steady-state solutions. Turbulence is modeled using an algebraic mixing length formulation to compute the turbulent eddy viscosity. The Navier-Stokes equations are discretized on a nonorthogonal mesh consisting of body-fitted J lines and vertical I lines. Reference 1 contains further details concerning the solution algorithm employed in code P367.

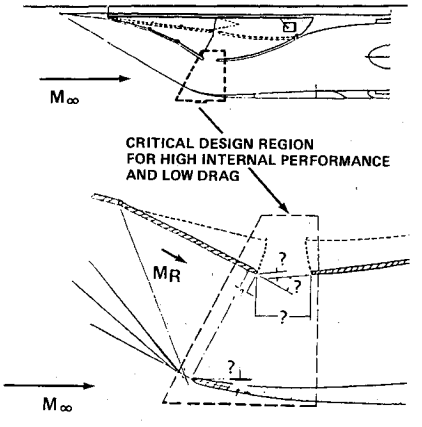

Fig. 1 Critical design region of a high Mach two-dimensional external compression inlet.

Code P367 required modifications to simulate the inlet aperture region geometry and boundary conditions. The modifications included the addition of a mass flux exit boundary condition, the capability to handle three different boundary conditions on the ramp wall, and additional mesh expansion capability. In addition, a procedure was incorporated for averaging the artificial viscosity terms required by the explicit MacCormack algorithm for stability. The third-order artificial viscosity or damping in code P367 is proportional to the change in pressure gradient. As disturbances move through the flowfield, the pressure distribution is perturbed, causing the artificial viscosity to grow. As disturbances are damped out, the artificial viscosity decays proportionally with the change in pressure gradient. The averaging procedure slows the rate of the decay of the third-order damping term. Whenever the instantaneous damping becomes larger than the average, the instantaneous value is used. This technique for slowing decay without hindering the growth of the artificial viscosity terms circumvented a limit cycling problem encountered early in the investigation. Finally, a fixed I/J-direction time step ratio was added to code P367. The explicit MacCormack algorithm employed in P367 splits I- and J-direction calculations to permit multiple sweeps in the direction that is limited by stability criteria to a smaller step size. A situation was encountered during this investigation where the ratio of sweeps in one direction to

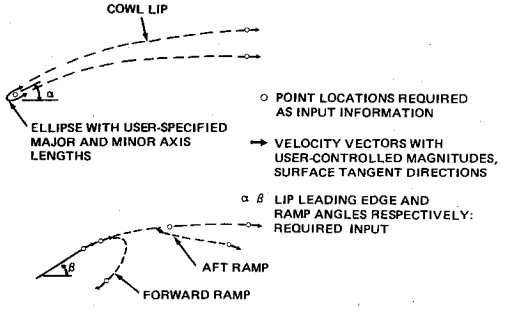

Fig. 2 Mechanics of ECIG aperture region geometry generation.

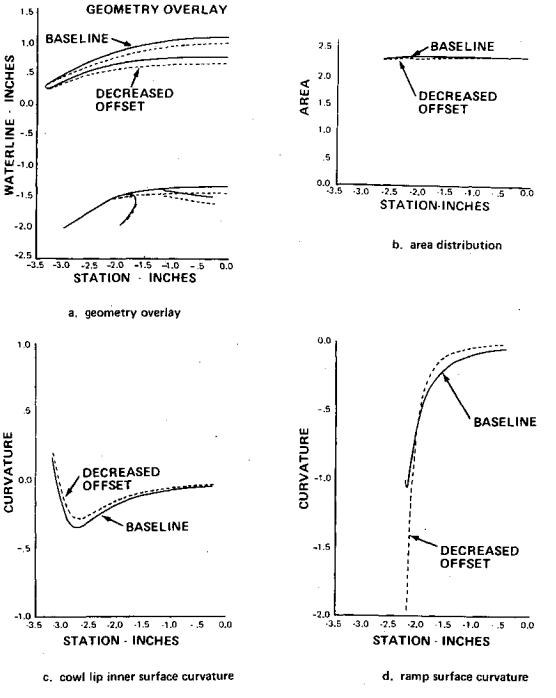

Fig. 3 Comparison of two inlet aperture region geometries generated using ECIG.

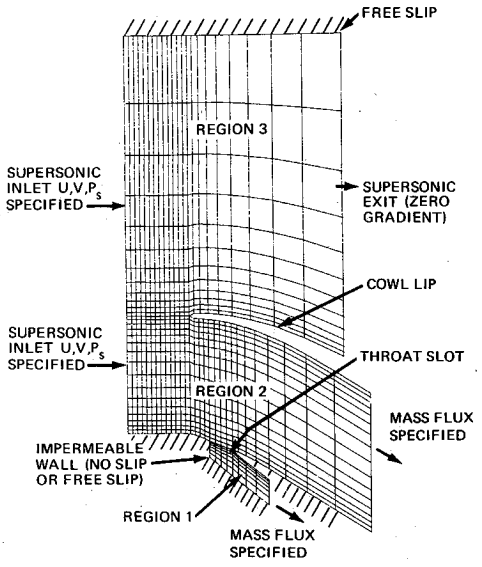

Fig. 4 P367 aperture region boundary conditions shown on a representative inviscid mesh.

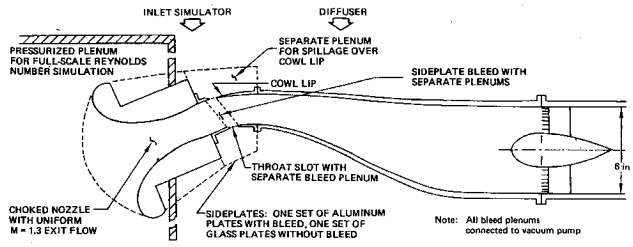

Fig. 5 Diffuser apparatus.

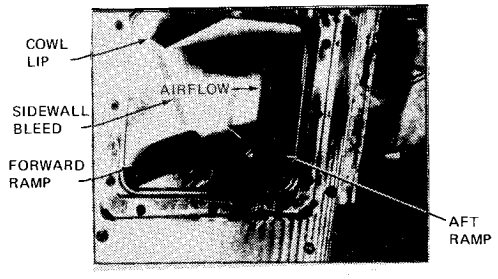

Fig. 6 Inlet simulator.

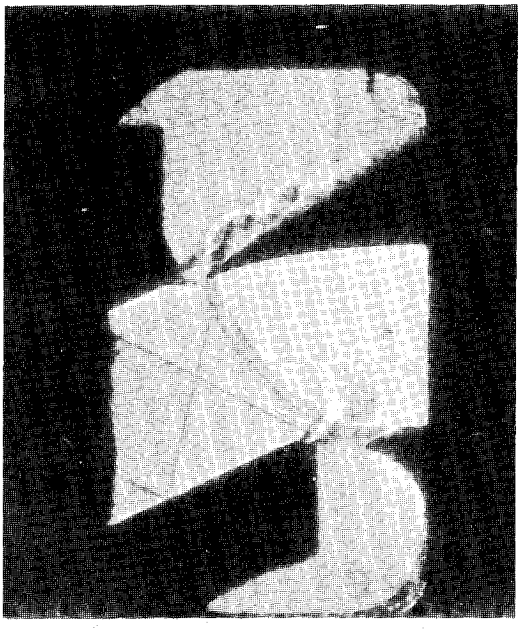

Fig. 7 Shadowgraph of 0.5% supercritical normal shock.

those in the other direction alternated between two values. This also resulted in a limit cycle preventing convergence. The ratio of I- to J-direction sweeps is now fixed after some arbitrary number of cycles.

Code P367 is capable of modeling up to three regions. Divisions between regions occur where inlet and/or exit boundary conditions change. The program allows cross flow or strong interaction boundaries between regions as well as hard-wall, no-slip, or free-slip boundaries within a region. The size of the computational mesh is defined by the user. The code internally generates a nonorthogonal mesh based on input information defining surface coordinates, region divisions, and mesh size. Boundary conditions used in the current study are illustrated in Fig. 4. Wall functions based on a compressible law of the wall velocity profile for turbulent boundary layers are used at all no-slip, solid-wall boundaries to reduce the number of cells required to define the boundary layer. This improves the computational efficiency by reducing both the computer storage requirements and the number of cycles required to achieve reasonable residual tolerances.

Solution convergence is judged based on residual level (defined here as changes in pressure and x-direction velocity over a 10 cycle period at specific locations in the mesh) and on change in spillage mass flow with cycle number. Convergence history, surface pressure distribution, boundary-layer profile, velocity vector, and Mach number contour plots can be generated from P367 output.

III. Validation Data

Validation studies of P367 conducted thus far have used a previously designed Mach 2.5 two-dimensional external compression inlet as the baseline configuration. The aperture region of this inlet has been experimentally evaluated in the test apparatus described in Ref. 4 and discussed briefly below.

A schematic of the test apparatus is presented in Fig. 5. A high-pressure plenum supplies air to a two-dimensional nozzle that expands the flow to a uniform Mach number of 1.3. A two-dimensional "inlet simulator" section is installed just downstream of the nozzle. The inlet simulator is designed just like the lip and throat section of a two-dimensional external compression inlet. Critical features, such as the normal shock/boundary-layer interaction on the ramp and the sideplates, flow spillage around the cowl lip, flow removal through the throat slot, sideplate bleed in the vicinity of the normal shock, and the flow turning through the forward part of the inlet are simulated with this test setup. Three separate vacuum lines are provided to allow individual control of the pressures in the lip spillage plenum, throat slot bleed plenum, and sideplate bleed plenums.

The primary objective of this test apparatus is to provide realistic flow conditions for evaluation of subsonic diffusers. The diffuser to be tested is installed just downstream of the inlet simulator as it would be on the actual inlet. A 6 in. diameter rotating rake is mounted at the diffuser exit to measure the total pressure flow profiles at the simulated engine face. Flow straighteners, flow metering devices, and a hydraulically actuated mass flow plug are connected to the downstream end of the rotating rake assembly.

In addition to providing representative diffuser entrance conditions, the test apparatus also allows investigations of the effects of normal shock position, throat slot bleed, and sideplate bleed on the diffuser performance. These capabilities are illustrated in Figs. 6 and 7.

The only appreciable losses for a two-dimensional external compression supersonic inlet not simulated with the test apparatus are the oblique shock losses upstream of the normal shock. When these losses can be accurately predicted, the performance results from tests in this apparatus can be applied to an actual supersonic inlet with a high degree of confidence.

The inlet aperture configuration used as the baseline for the present analytical study has already been evaluated in the diffuser test apparatus. Figures 8-10 illustrate the type of data available.

IV. Analysis Results

Analysis code P367 has been run extensively in an inviscid mode for two-region (no bleed slot) and three-region simulations. In addition, several two-region viscous runs were made before extending the analysis to include three-region viscous flow. The inviscid runs provided a cost-effective means of verifying that the code could indeed model inlet geometry and boundary conditions. In addition, valuable information was obtained concerning the levels of artificial viscosity required and the value of the multiplier on the maximum time step computed from stability analysis, i.e., the CFL number.

Two-Region Study Results

The two-region viscous runs were used to conduct a grid refinement study and to study the effect on the ramp wall pressure distribution of varying the cowl lip spillage flow. The grid refinement study was conducted to identify the level of resolution required to adequately model for preliminary validation studies the shock/boundary-layer interaction on the ramp wall. Grid resolution was judged adequate when the ramp wall pressure distribution ceased to change appreciably with increasing mesh refinement. A summary of the five grids studied is provided in Table 1. In all cases, the mesh was expanded in the J direction out from the walls at a 20% rate. No expansion was permitted in the I direction from the left boundary to the cowl lip in either region. Additionally, in region 2, no expansion was permitted from the lip to what would be the leading edge of the aft ramp in a three-region study. These restrictions on I direction expansion prevented unnecessary smearing of the discretized shock.

The first two grids tested represented a refinement in J-direction spacing. Mach number contour plots and ramp wall pressure distributions are presented in Fig. 11. Predictably, little was gained in terms of ramp wall pressure distribution since this test will be influenced more by I-direction refinement. In addition, the I-direction mesh was probably too coarse at this stage to learn much from J-direction refinement. Further study of the effect of J-direction refinement at an increased level of I-direction resolution is planned.

The last four grids tested represented refinements in I-direction spacing for constant J-direction spacing. Mach number contour plots illustrating the increased resolution of the shock with grid refinement are shown in Fig. 12. Figure 13 is a comparison of ramp wall pressure distributions for the four different I-spacing grids. The ramp wall pressure distributions clearly show the shock impinging on the ramp wall upstream of the curvature-induced expansion. A second shock impinges on the wall downstream of the expansion. The location of the second shock was probably influenced by the inclusion of the bleed slot geometry in the two-region simulations. Although the geometry defining the forward ramp and aft ramp components remained in the simulation, the boundary condition across the slot opening was set for an impermeable wall with no slip. A blowup of the mesh in the region of the bleed slot for the eight-cell between-lip-and-slot grid is contained in Fig. 14. The wall closing off the throat slot opening is simply a straight-line connection from

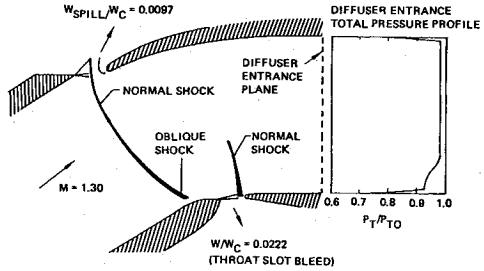

Fig. 8 Diffuser entry performance.

Fig. 9 Interferogram of diffuser entry flowfield.

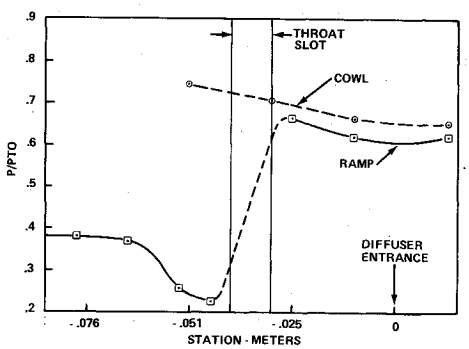

Fig. 10 Static pressure distributions along ramp and cowl surfaces.

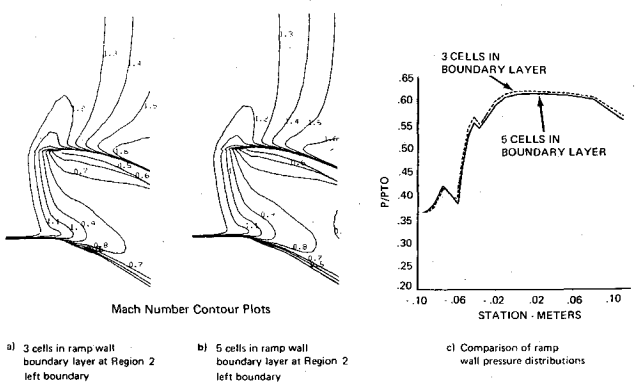

Fig. 11 J-direction grid refinement.

the end of the forward ramp to the lip of the aft ramp. A change in slope occurs where the forward ramp ends and the straight-line connection begins. Clearly, this change in slope will compress the supersonic flowfield and generate a shock, thereby influencing the location of the shock that must occur after the expansion on the forward ramp surface. The sharp pressure rise and fall shown in Fig. 13 at station -0.042 results from compression and expansion of the flow around the leading edge of the aft ramp located at that station.

Inspection of Fig. 12 reveals that dramatic improvement in shock resolution was achieved in going from two to four cells in the region between the lip and slot opening. The step change in resolution appears to decrease between the 4 and 8 cell grids and again between the 8 and 16 cell grids. Figure 13 reveals similar results in terms of shock resolution but high- and low-pressure values do change substantially between the 4 and 8 cell grids and then again between the 8 and 16 cell grids. This is particularly true of the low-pressure point at station -0.06. These results suggest that further mesh refinement is warranted for obtaining all of the subtle surface pressure features. Nevertheless, shock resolution was judged adequate with the 8 cell between-lip-and-slot grid for studying the effect of decreased spillage flow on ramp wall pressure distribution. High- and low-pressure level definition was sacrificed in deference to cost efficiency. The 16 cell between-lip-and-slot grid was chosen for the three-region viscous simulation.

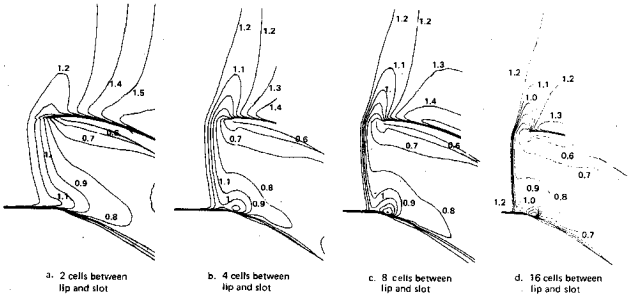

Fig. 12 *I*-direction grid refinement results: Mach number contour plots.

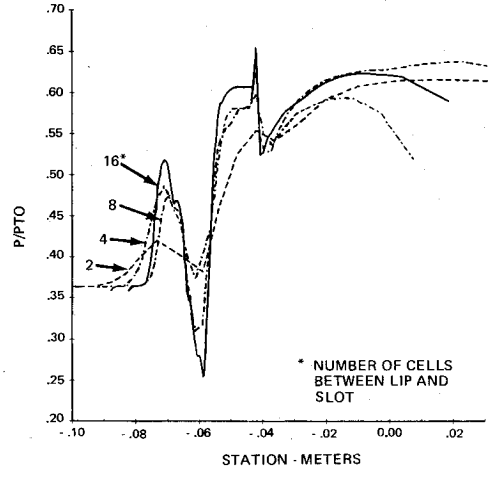

Fig. 13 *I*-direction grid refinement results: ramp wall pressure distribution.

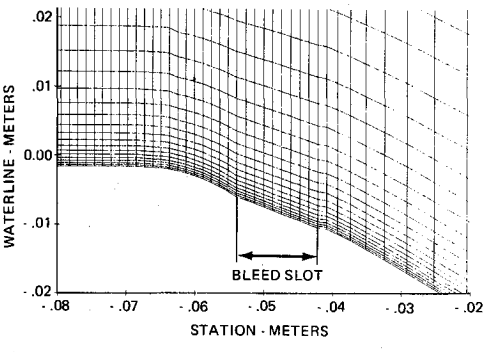

Fig. 14 Blowup of 54×38 region 2 mesh showing bleed slot geometry representation for two-region simulations.

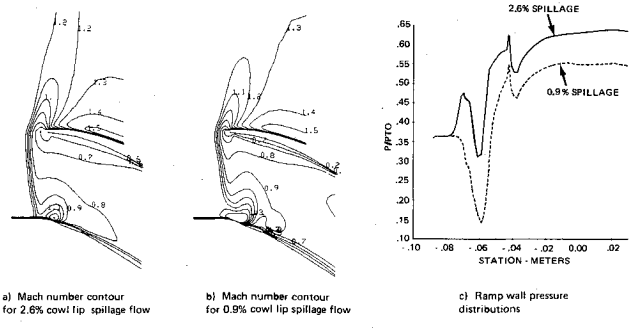

Fig. 15 Comparison of analytical results for 2.6 and 0.9% subsonic cowl lip spillage flow.

Table 1 Results of two-region, 2.6% spillage rate grid refinement study

Mesh size, $I \times J$ (region 2) (region 3)	No. of cells between lip and beginning of slot	No. of cells in ramp wall boundary layer at left boundary	No. of steps to convergence	Computer time, min
29×32 27×20	2	3	5,000	16.1
29×38 27×22	2	5	7,000	28.3
38×38 32×22	4	5	7,000	37.5
54×38 34×22	8	5	18,000	79.0
80×38 42×22	16	5	14,000[a]	68.7

[a]Started with initial condition equal to results of a 10,000 step simulation of a 0.9% spillage rate.

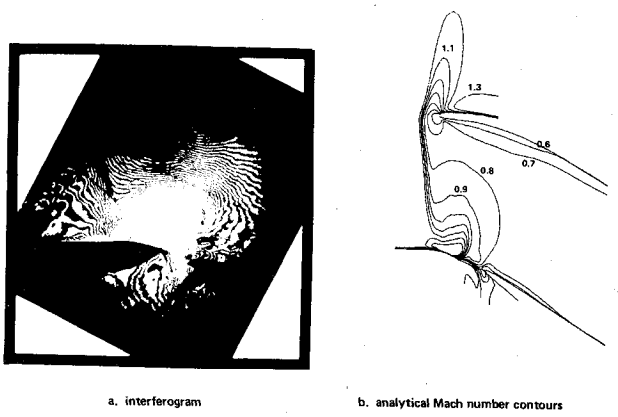

Fig. 16 Comparison of analytically generated Mach number contours with interferogram data.

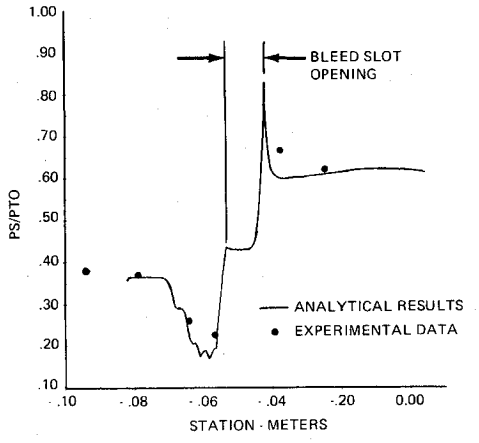

Fig. 17 Ramp wall pressure distribution: comparison of analytical results with experimental data.

The above grid refinement study was done for a cowl lip spillage flow equal to 2.6% of the capture mass flow. A 0.9% spillage simulation was done to study the change in pressure distribution along the ramp wall resulting from the movement of the shock for the reduced spillage mass flow. A comparison of Mach number contours and ramp wall pressure distributions is presented in Fig. 15. The normal shock has moved closer to the lip for the lower spillage flow and no longer extends across the inlet entry plane to the ramp wall. The normal shock that occurs directly downstream of the curvature-induced expansion is, however, located at the same position for both spillage flow rates. This is probably due to the presence of the throat slot geometry as explained earlier. From this point on downstream, the shape of the two ramp pressure distributions is essentially the same, but the levels are shifted everywhere, reflecting the increase in primary airflow resulting from the lower spillage mass flow of the 0.9% cowl lip spillage run. The presence of the bleed slot geometry has undoubtedly affected the results of this study; nevertheless, it is clear that information of this nature is what is required to size and locate the bleed slot opening.

Three-Region Validation Study Results

Validation of the analysis is still in the initial stages. A comparison of analytical results with experimental data generated at the Boeing Diffuser Test Facility for one inlet geometry at one operating point is given. The cowl lip and ramp wall geometries are the same as used in the above two region studies. A third region (denoted region 1) was added

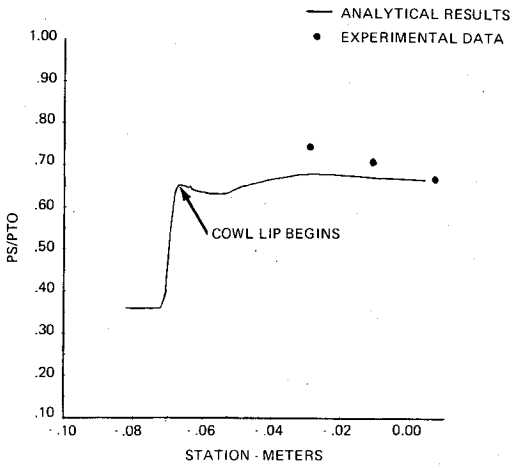

Fig. 18 Cowl lip surface pressure distribution: comparison of analytical results with experimental data.

to serve as the throat slot bleed plenum. The analysis flowfield boundary conditions were chosen to match as nearly as possible test conditions for the experimental data that were presented in Figs. 8-10. Thus, the simulation is for a bleed flow equal to 2.22% of the capture mass flow with a cowl lip spillage flow of 0.97%.

The mesh consisted of 29×12, 80×38, and 42×22 cells in regions 1-3, respectively. The solution required 124 min of CRAY I computer time to converge. This represented 24,000 cycles.

A Mach number contour plot generated from the analysis is compared with experimental data in the form of an interferogram in Fig. 16. The interferogram depicts lines of constant density. The overall similarity between the analytical results and the experimental data is very encouraging. The bow shock just off the cowl lip is positioned in nearly the same location. The numerical shock, however, exhibits less curvature than the experimental shock, so that discrepancies in shock location grow in moving from the cowl lip toward the ramp wall. More significantly, the normal shock that occurs near the leading edge of the aft ramp in the experimental data is shifted forward by approximately 70% of the length of the bleed slot in the numerical simulation. The discrepancy is probably due to a throat slot plenum pressure in the numerical simulation that is nearly twice the plenum pressure that existed during the experiment. The analytical throat slot plenum pressure is also roughly twice the pressure on the forward ramp surface just upstream of the throat slot opening. This is illustrated in Fig. 17 where the pressure across the initial part of the bleed slot opening is nearly equivalent to the plenum pressure. A strong oblique shock occurs at the beginning of the throat slot opening in order to establish equilibrium. A strong, largely subsonic compression occurs near the leading edge of the aft ramp that nearly coincides with the location of the shock in the experimental data.

The discrepancy in throat slot plenum pressure probably results from the way the throat slot plenum is simulated in the analysis. Further study of the effect of varying the simulated plenum volume, the location of the left and right walls, and the manner in which mass flow exists the plenum is required for a more complete understanding.

Ramp wall and inner cowl lip surface pressure distributions generated from analysis are compared with experimental data in Figs. 17 and 18, respectively. Figure 17 reveals that ramp wall surface pressure data are well predicted in this case. The greatest discrepancy occurs at station -0.038 where the numerical result is 10% lower than the experimental data. The cowl lip surface pressure distribution is also predicted within 10% but the scarcity of data prohibits conclusive evaluation.

V. Conclusions

Significant progress has been made toward the development of an analytical design procedure for the aperture region of external compression supersonic inlets. The geometry generation code has already been used to design several aperture region geometries for an upcoming test at the Boeing Diffuser Test Facility. Results from the upcoming experimental investigation as well as additional operating points for the baseline aperture region geometry will be used to complete validation of the analysis approach described in this paper. One very notable advantage of the approach employed here is that solutions generated for a particular size mesh may be used as the initial condition for any future simulations involving the same mesh size but for which boundary conditions or even geometry descriptions may vary. This will in most cases greatly reduce the number of steps required to reach convergence and thus reduce the cost of future analyses.

References

[1]Peery, K. M. and Forester, C. K., "Numerical Simulation of Multistream Nozzle Flows," *AIAA Journal*, Vol. 18, Sept. 1980, pp. 1088-1093.

[2]Peery, K. M. and Russell, D. L., "A Numerical Investigation of Exhaust Plume Temperature Effects on Nonaxisymmetric Nozzle/Afterbody Performance," Paper presented at AGARD Symposium on Aerodynamics of Power Plant Installations, Toulouse, France, May 11-14, 1984.

[3]Kowalski, E. J., Peery, K. M., and Klees, G. W., "Numerical Simulation for the Design of a Supersonic Cruise Nozzle with Fluid Noise Shield," AIAA Paper 81-1218, June 1981.

[4]Syberg, Jan and Koncsek, Joseph, "Performance Variations in High Aspect Ratio Subsonic Diffusers Due to Geometric Constraints in Supersonic Tactical Aircraft Inlet Installations," AIAA Paper 80-1106, June 1980.